Mathematical & Computational Applications, Vol. 8, No. 2, pp. 225-233, 2003

APPLICATION OF NEURAL NETWORKS TO ESTIMATE COMMON MODE (CM) MODEL IMPEDANCE PARAMETERS IN AC DRIVES

Kayhan Gulez and Nobuyoshi Mutoh
Tokyo Metropolitan Institute of Technology,
Department of Electronic Systems Engineering
6-6 Asahigaoka Hino-Shi, 191-0065, Tokyo, JAPAN
kgulez@cc.tmit.ac.jp, nmutoh@cc.tmit.ac.jp

Abstract- Predicting and solving EMI emissions related to Common Mode (CM) ones in inverter (including pulse with modulation (PWM) inverter)-induction motor drive systems requires various frequency-dependent effects to be considered. Thus, the application of filter circuitry to improve the performance per size and prevent dependency on some parameters of the motor for Electro-Magnetic Interference (EMI) filter is considered. The major problems are power line frequency rejection and the compensation of the feedback loop, which is influenced by the wide-ranging utility impedance. Thus, the proposed method allows another way to determine Common Mode (CM) impedance components as a beginning way and sample on the application stage of EMI filter to prevent the EMI noise applying to the conducted electromagnetic emissions generally caused by power supply firstly, then secondly to Common Mode (CM) path of the motor drive system.

Keywords: EMC/EMI, AC Drives, Neural networks, Common Mode (CM) impedance.

1. INTRODUCTION

The common and differential mode excitation sources are easily modeled in the frequency model and related to switching functions of the PWM inverter. Network models are used where the induction motor is represented using its frequency-dependent impedance characteristics. The power electronic devices rapidly spread with the advance for electric power and high speed processors in our daily technology. The conducting emission with the switching condition which was not being taken up by now becomes a large problem tangibly. The effect of the conducting emissions broadens electric power system and gives dependence to the parameters of the main devices or filters as a failure to the peripheral equipment [1]-[3]. As differential mode oscillations between output phases tend to be in the megahertz range, it is only necessary to consider a detailed motor model for the common mode emissions. Thus, we are now concerning with not only low-frequency range but also HF band of interest up to 3 MHz. Common Mode impedance (between motor terminals and frame) is affected by the rotor speed and position. It has to be analyzed for some special applications. EMI noises of the motor drive system shown in Figure 1 are studied. From this point of view, this paper is especially based on the new approach which uses ANN approximation to an initial study of determining HF Common Mode (CM) impedance of the drive system. For both delta and star connections, the common mode impedance can be expressed as a function of the frequency,

$Z_{mot}(w) = R_{mot}(w)+jX_{mot}(w)$ (1).

Equ. 1 indicates that every switching event in the inverter (even if it is a PWM one) will produce a disturbance in the Common Mode (CM) circuit.

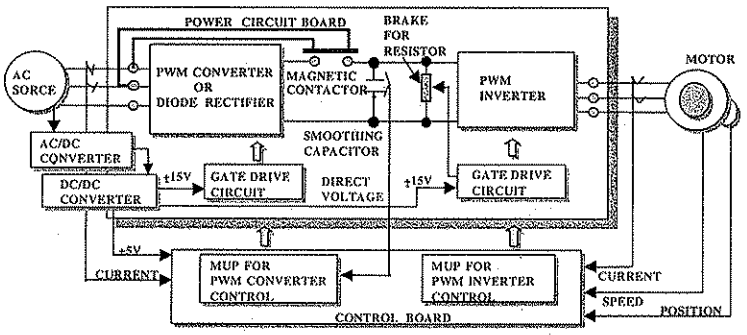

Figure 1. Structure of motor drive system using a printed circuit board

2. EMI EMISSIONS OF MODERN AC DRIVES

Electromagnetic Interference (EMI) noise is defined as an unwanted electrical signal that produces undesirable effects in a control system, such as communication errors. All AC drives (including PWM ones) have the potential to cause EMI with adjacent sensitive equipment, when large quantities of drives are assembled in a concentrated area [4]-[8]. However, faster switching speeds of new converter/inverter topologies require an updated study of new system EMI issues [9]-[13]. Increasing drive quantity increases the sum total of transient CM noise current to ground. Higher drive carrier frequency increases the number of switch transitions and sum total of transient CM noise current.

In the case of EMI mitigation, it is important to determine protection equipment ground, signal grounding and the effect of grounding system type on CM noise. Common Mode (CM) conducted emissions are due to currents which flow between the input phases and the earth of the system [5], [6]. In a drive system, they are principally due to the combination of the rapidly switched inverter output voltage and the various stray capacitances to earth at the output side of the drive. A generic equivalent circuit for the common mode currents can be developed by making suitable assumptions. At the input side of the drive, the 3-phase of the Double-LISN (Line Impedance Stabilization Network) [9] and input cable are connected in parallel with respect to the earth. The high frequency component is blocked by the inductance of the Differential Mode (DM) filter and is therefore constrained to flow mainly through the stray capacitance between the power circuit and the heat sink. This leads to the High Frequency Common Mode (CM) equivalent circuit (general diagram in Figure 2 with current paths in Figure 3). At this frequency, the induction machine can be represented simply by its terminal capacitance since there is little or no penetration into the winding. Resistances $R_{d1\text{-}d2}$ are included to model damping (loss) effects due to the cable. Suitable values are difficult to determine directly, but can be deduced by comparing simulation results and experimental measurements. The un-dumped oscillation

frequency (f_{cm1}) of the circuit can be derived from the total series inductance (L_{cm1}) and capacitance (C_{cm1})

$$f_{cm1} = \frac{1}{2\pi\sqrt{L_{cm1}C_{cm1}}} \quad (2)$$

[10], [11], where (L_{cm1}) and (C_{cm1}) can be expressed as follows;

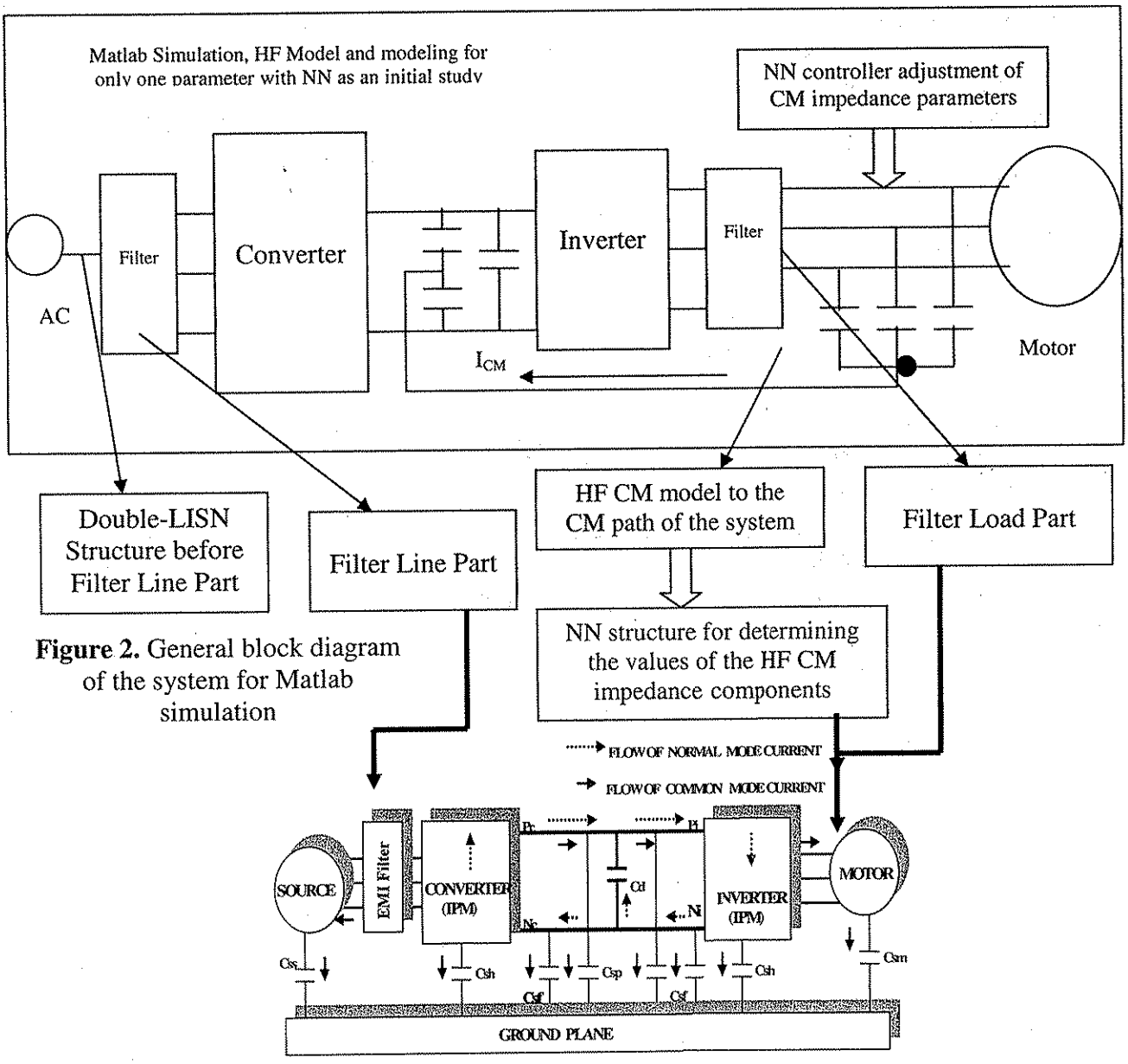

Figure 2. General block diagram of the system for Matlab simulation

Figure 3. Normal mode current supplying electric power to a motor, and paths of common mode currents flowing through stray capacitors formed on the power circuit.

$$L_{cm1} = 4\,L_{cab} \quad (3)$$

$$C_{cm1} = [C_{stray} + (3/2)C_{cab2}][6C_t + (3/2)C_{cab2}] / (C_{stray} + 6C_t + 3C_{cab2}) \quad .(4)$$

From our system equations, It is calculated that L_{cm1} is 30 nH and C_{cm1} is 4773 pF. From the calculations on the equations 4 and 5, L_{cab2} = 22.5 nH, C_{stray} = » 9* 4773 pF, (9*C_{cm1}), C_{cab2} = 1 nF, C_t = 14.4 nF (represents adequately the motor impedance in such cases of inter phase oscillations in the high frequency range), R_{d1} and R_{d2} are included to model damping effects due to the cable. Suitable values are difficult to determine directly, but can be deduced by comparing simulation results and experimental measurements. Here, they are 0.1 Ohm according to the condition. Since the high frequency mode is mainly trapped between the IGBT inverter and the induction motor, its contribution to the total conducted emissions measured at the LISN is not significant. However, depending on the drive system arrangement in practice, it may disturb other equipment by various means of cross talk [7], [8], [11], [12], [14]. Figures 2-5 show a simplified representation of a general system block diagram including NN controller, the figure of current paths of the system, HF Common Mode (CM) frequency domain equivalent circuit and single phase schematic of Double-LISN respectively.
The general mathematical conditions of LISN part as follows;

$$A = \begin{bmatrix} 1 & 0 \\ \dfrac{R_1 + JX_{c1}}{R_1^2 + X_{c1}^2} & 1 \end{bmatrix} \begin{bmatrix} 1 & JX_{l1} \\ 0 & 1 \end{bmatrix} \begin{bmatrix} 1 & 0 \\ \dfrac{R_2 + JX_{c2}}{R_2^2 + X_{c2}^2} & 1 \end{bmatrix} \tag{5}$$

$X_{c1} = 1/(2pKfC_1) = 1.768/K$
$X_{l1} = 2pKfL_1 = 1.407\ K$
$X_{c2} = 1/(2pKfC_2) = 1.768/K$

related to the solution type of the equation

$$\begin{bmatrix} A + JB & C + JD \\ E + JF & G + JH \end{bmatrix} \tag{6}$$

f, frequency, K, the normalized frequency, which has the value of 1 at the cut-off frequency. After solving the letters A to H [26], according to the value of frequency, the component values of LISN circuit are easily determined (in Figure 5).

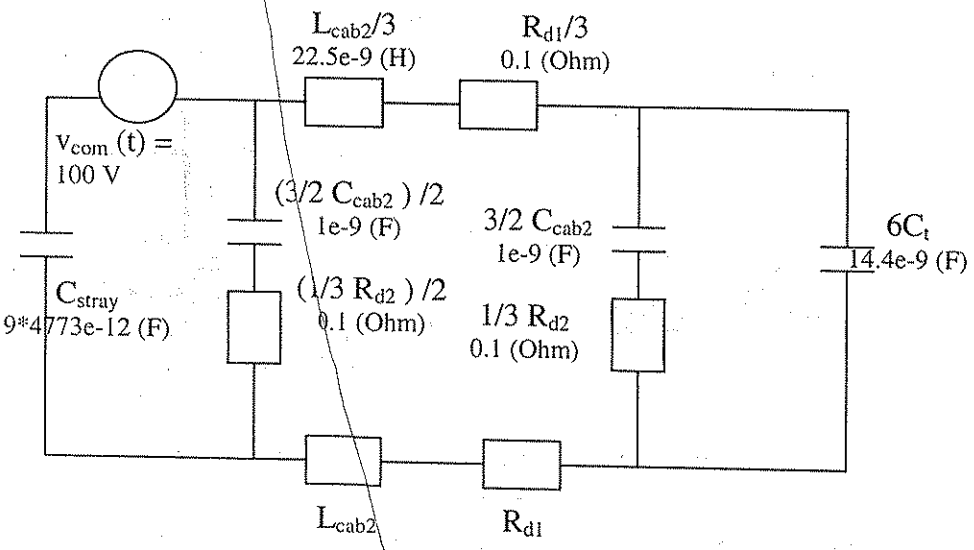

Figure 4. High frequency common mode (CM) equivalent circuit

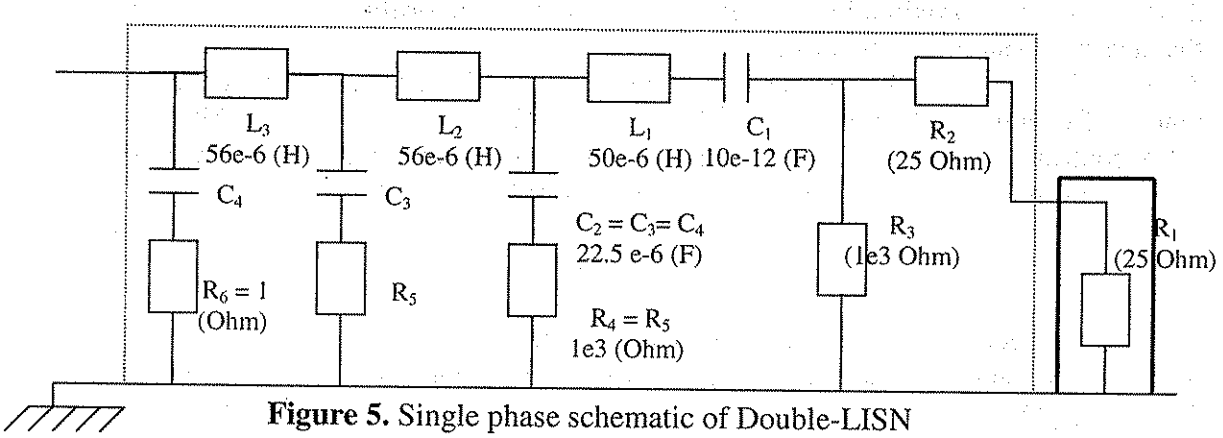

Figure 5. Single phase schematic of Double-LISN

3. FAST BACKPROPAGATION ALGORITHM

This algorithm is derived by sequentially minimizing the objective function $G_k(\lambda)$, defined by equation 7, for k=1,2,.....m. The update equation for the synaptic weights w_{pq} is obtained as equation 8.

$$G_k(\lambda)=\lambda\sum_{i=1}^{n_0}\phi_2(e_{i,k})+(1-\lambda)\sum_{i=1}^{n_0}\phi_1(e_{i,k}) \quad \forall k=1,2,.....,m \qquad (7)$$

$$w_{p,k}=w_{p,k-1}+\alpha\varepsilon^0_{p,k}(\lambda)\hat{h}_k \qquad (8)$$

Here, $\phi_2(x)=\frac{1}{2}x^2$ and $\phi_1(.)$ is a positive, convex and differentiated function at every place. $\lambda \in [0,1]$.

If the output of the network is analog,

$$\varepsilon^0_{p,k}(\lambda)=\lambda(y_{p,k}-\hat{y}_{p,k})+(1-\lambda)\tanh\left[\beta(y_{p,k}-\hat{y}_{p,k})\right] \qquad (9)$$

$\sigma(x)=x$ and $\sigma'(x)=1$. In this condition, it is determined $\phi_1(.)$, $\phi_1(x)=(1/\beta)$. From here, it is easy to understand $\phi'_1(x)=\tanh(\beta x)$ and $\phi_2(x)=1/2\ x^2$ ve $\phi'_2(x)=x$.

On the other hand, if the network has binary outputs,

$$\varepsilon^0_{p,k}(\lambda)=(1-\hat{y}^2_{p,k})(y_{p,k}-\lambda\hat{y}_{p,k}) \qquad (10)$$

Because of its simplicity and speed, this algorithm provides an ideal basis for investigating the role of λ during training. Here, $\varepsilon_{p,k}$ and α are the output error and learning rate respectively. λ is given as,

$$\lambda=\exp(-\mu/E^2) \qquad (11)$$

where μ is selected by user with a cut and trial process on the training stage of the algorithm [15]. Utilization of neural networks provides the advantage of determining the component of CM in an easy way.

The advantages of using Fast Back-propagation algorithm are,

1- Fast results both in training and test phases comparison to the other ANN algorithms (as fast as nanoseconds),
2- Besides fast approximation as compared to the other algorithms, we may also claim that accurate results are obtained.
As an initial study, considering a simplest circuit with only one impedance related to the random frequency values between 0 kHz and 3 MHz, the associated architecture of ANN controller can be given as in Figure 6 and comparative diagram of the results can be given as in Figure 7. Table 1 shows test phase results of ANN.

4. CONCLUSIONS

A DynaBook Satellite 2060 computer is used to train NN controller. C++ is used as programming language for programming ANN. In the paper, for Fast Back-propagation Algorithm [15], Frequency (f) (in kHz) is used as the input to ANN, and Resistance (R_m) and Reactance (X_m) are the output quantities of ANN of the motor to apply the proposed method for the simplest circuit. The results are made and discriminated with success rate under %0.1 generalized system error. For 350000 iterations, the generalized system error is %0.0299 including 3 and 4 nodes in 2 hidden layers respectively. These results important success for improving the performance that is adapting to changes in a very short time (nanoseconds). In addition to all these, the simulator diagram of CM voltage control circuit including EMI filter with NN controller to the path of Common Mode in the Motor Drive System, (Matlab simulations [16], [17]), HF CM model voltage and current diagrams, CM voltage and leakage current simulation and experimental result diagrams of the system and the spectrum analysis results of them both in simulation and plots of experimental results are depicted in Figure 8 to Figure 13 respectively. As can seen from Figures 11 and 12, the results of the filter application simulations of the system are similar to the system requirements. The representation of the model parameters more than one with NN and the improvement of general circuit according to the system requirements are under consideration with spectrum analysis.

Acknowledgment
The research is carried out by the assist of research project "Control of Electromagnetic Environment in Low Frequency Band Less Than 100 kHz" of the reclamation research promotion business in the future of JSPS-Japan Society for the Promotion of Science. The authors are thankful for the assist of JSPS- Japan Society for the Promotion of Science.

REFERENCES

[1] Lin, F. and Chen, D.Y. "Reduction of Power Supply EMI Emission by Switching Frequency Modulation", *IEEE Trans. On Power Electronics*, Vol.9, No.1, pp. 132-137, January 1994.
[2]] Farkas, T. "Viability of Active EMI Filters for Utility Applications", *IEEE Trans. On Power Electronics*, Vol.9, No.3, pp. 328-336, May 1994.
[3] Walker, J. "*Designing Practical and Effective Active EMI Filters*", in Powercon 11 Proc., April 1984, Paper 1-3.
[4] Skibinski, G., Pankau, J., Sladky, R. and Campbell, J., "*Generation, Control and Regulation of EMI from AC Drives*", Proc. IEEE-IAS Ann. Conference, New Orleans, LA, pp. 1571-1583, October 2-6,1997.

[5] Ong, C.M., *Dynamic Simulation of Electric Machinery: Using Matlab/Simulink*, Prentice-Hall, New Jersey, 1998.
[6] Ran, L., Gokani, S., Clare, J., Bradley, K.J. and Christopoulos, C., "Conducted Electromagnetic Emissions in Induction Motor Drive Systems Part I: Time Domain Analysis and Identification of Dominant Modes", *IEEE Trans. on Power Electronics*, Vol.13, No.4, pp. 757-767, July, 1998.
[7] Ran, L., Gokani, S., Clare. J., Bradley, K.J. and Christopoulos, C., "Conducted Electromagnetic Emissions in Induction motor Drive Systems Part II: Frequency Domain Models", *IEEE Trans. On Power Elec.*, Vol.13, No.4, pp.768-776, July 1998.
[8] Paul, C.R. and Hardin, K.B., "Diagnosis and Reduction of Conducted Noise Emissions", *IEEE Trans. Electromag. Compat.*, Vol.30, No.4, pp.553-560, 1988.
[9] Gulez K., Nobuyoshi M., Harashima F. and Ohnishi K., "*A New Approach For Determining The Common Mode (CM) Impedance Parameters of EMI Emissions with The Fast Backpropagation Algorithm Of Neural Networks For Low Frequency Band*", IECON'2000, 22-28 October-2000, Nagoya-JAPAN.
[10] Gulez K., Watanabe H., Harashima F., Ohnishi K. and Pastacı H., "*ANN (Artificial Neural Network) Drive Controller of Space Vector Modulation Increasing The Performance of The Induction Motor And Ensuring Harmonic Reduction*", SICE'2000, 26-28 July-2000, Iizuka-JAPAN.
[11] Mutoh, N., Shirakawa, S., Komatu, K., Ohnuma, N. Hokari, S. and Harashima, F., "*Electromagnetic Characteristics of a High Density Motor Drive System Using Printed Power Circuit Board*", Trans. IEE of Japan, Vol.121-D, pp. 111-117, 2001.
[12] Gulez K., Mutoh N., Harashima F., Ohnishi K. and Uzunoglu M., "*Determining of HF CM Model Parameters with ANN for EMI Emissions*", EPE'2001, 27-29 August-2001, Graz-AUSTRIA.
[13] Mutoh N., Ogata M., Gulez K. and Harashima F., "New Methods to Suppress EMI Noises in the Motor Drive System", *IEEE Trans. on Industrial Electronics*, Vol.49, No.2, April-2002.
[14] Ozenbaugh, R.L., *EMI Filter Design*, Marcel Dekker Inc., 1996.
[15] Karayiannis, N.B. and Venetsanopoulas A.N., *Artificial Neural Networks- Learning Algorithms, Performance Evaluation and Applications*, Kluwer Academic Publishers, 161-195, 1994.
[16] *Matlab-6 version*, The Math Works Inc. ©, September-2000.
[17] *Matlab Power System Blockset User's Guide*, The Math Works Inc., January 1998, 1st Printing.

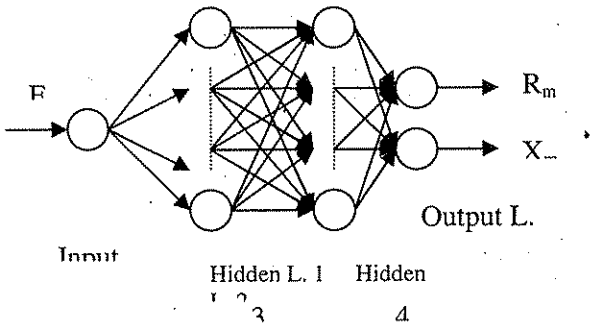

Figure 6. The architecture of NN

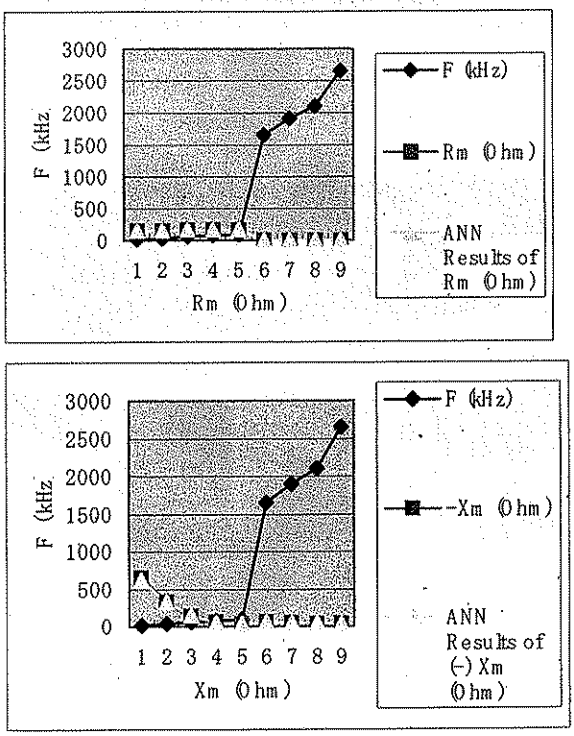

Figure 7. Comparative diagram of R_m and X_m with ANN results

Table 1. Test phase results of ANN

F (kHz)	R_m (Ohm)	$-X_m$ (Ohm)	ANN Results of R_m (Ohm)	ANN Results of (-) X_m (Ohm)
15	152	650	151.704	612.37
30	157	330	157.014	324.28
60	166	140	164.394	141.57
75	169	60	169.182	45.21
90	173	35	173.052	31.24
1650	0	55	0.370	54.07
1900	0	45	0.178	44.93
2100	0	38.5	0.115	40.27
2650	0	30.25	0.058	33.82

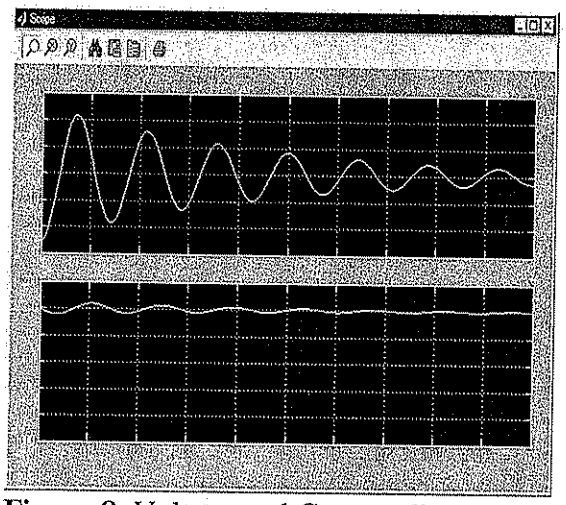

Figure 8. Voltage and Current diagrams of HF CM model

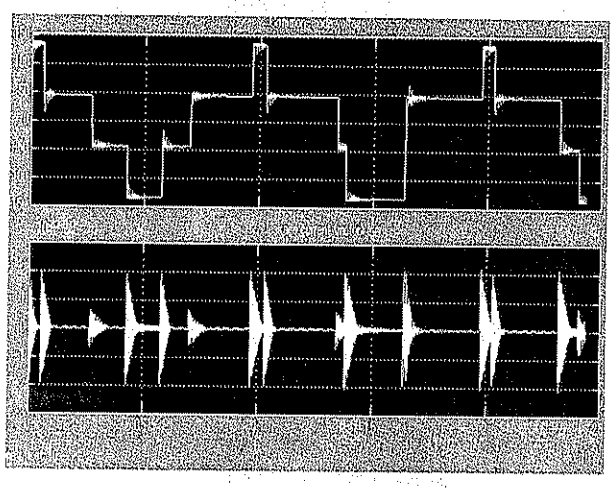

Figure 9. (a) CM voltage and leakage current simulation result diagrams of the system

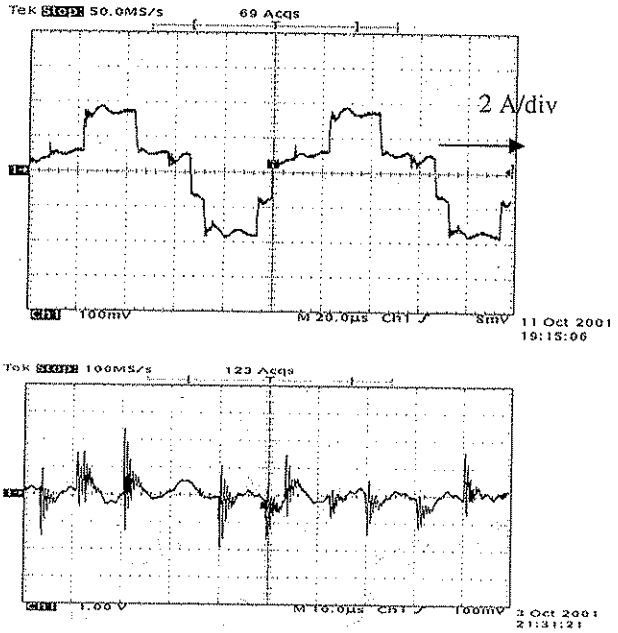

Figure 9. (b) CM voltage (c) Leakage current diagrams of the experimental system

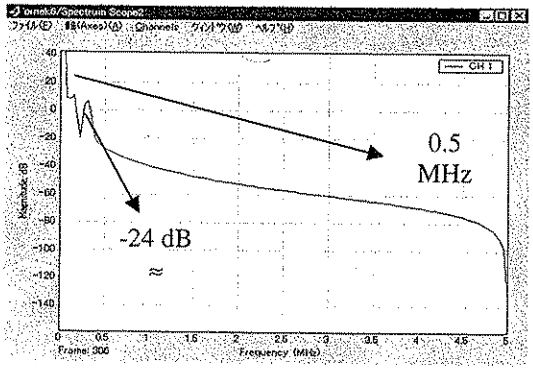

Figure 11. (a) The spectrum analyzer result showing noise condition before filtering taken from CM voltage path

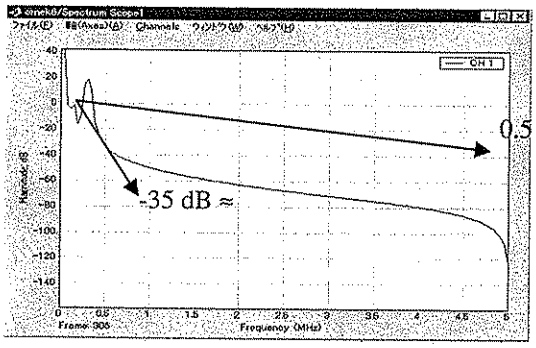

Figure 11. (b) The spectrum analyzer result showing noise condition after filtering taken from CM voltage path

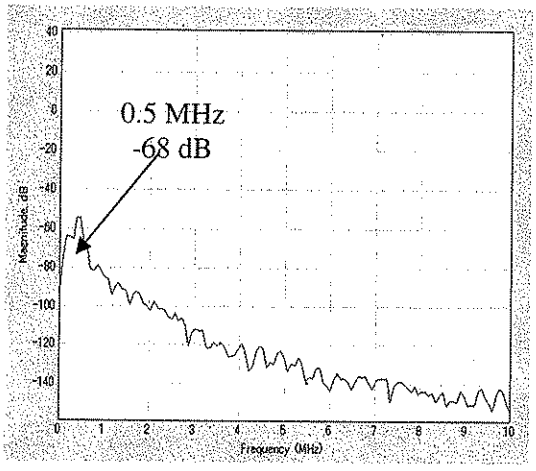

Figure 12. (a) FFT analysis diagram for the simulation result of the leakage current

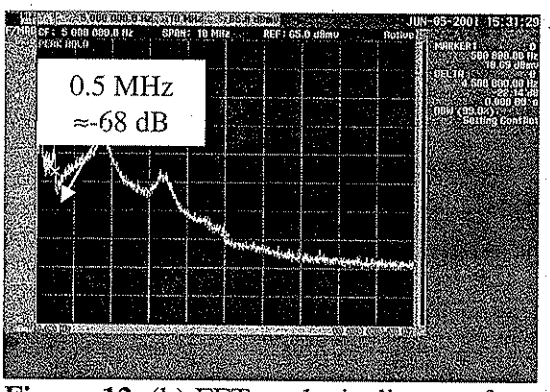

Figure 12. (b) FFT analysis diagram for the experimental system result of the leakage current

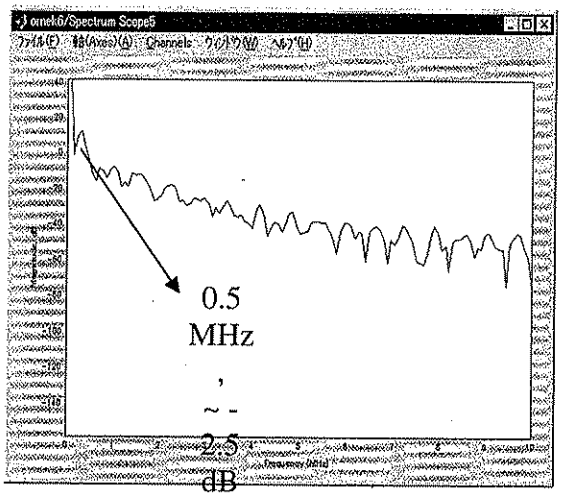

Figure 13. (a) CM Voltage, Simulation-FFT Motor Terminal side

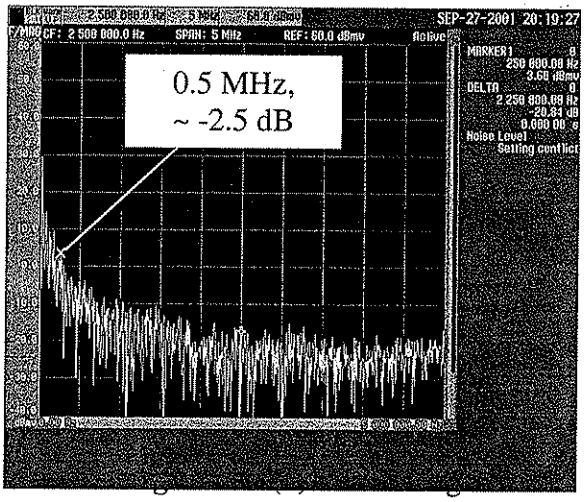

experimental result, FFT Motor Terminal side